Available online at www.sciencedirect.com
SCIENCE DIRECT®
Journal of Power Sources 119–121 (2003) 649–653
JOURNAL OF POWER SOURCES
www.elsevier.com/locate/jpowsour

^{6}Li MAS NMR and in situ X-ray studies of lithium nickel manganese oxides

Won-Sub Yoon[a,b], Namjun Kim[a], Xiao-Qing Yang[b], James McBreen[b], Clare P. Grey[a,*]

[a]*Department of Chemistry, State University of New York at Stony Brook, Stony Brook, NY 11794-3400, USA*
[b]*Brookhaven National Laboratory, Upton, NY 11973, USA*

Abstract

In situ XRD and ^{6}Li MAS NMR spectroscopy have been carried out during the first charge process for the layered cathode material $Li[Li_{1/9}Ni_{3/9}Mn_{5/9}]O_2$. In situ XRD results showed that the c-parameters of the $Li[Li_{1/9}Ni_{3/9}Mn_{5/9}]O_2$ material increase only slightly at the end of charge. The Mn and Ni K-edge EXAFS results revealed that this compound contains localized clusters resembling the local environments found in Li_2MnO_3 and lithium nickel oxide. The ^{6}Li MAS NMR results showed the presence of Li in the Ni^{2+}/Mn^{4+} layers, in addition to the expected sites for Li in the lithium layers. All the Li ions in the transition metal layers are removed on the first charge, leaving residual lithium ions in the lithium layers.

Keywords: ^{6}Li MAS NMR; In situ XRD; XAS; Lithium nickel manganese oxide; Battery

1. Introduction

$LiCoO_2$ is the most widely used cathode material in commercial secondary lithium batteries as it is easy to prepare and has a high theoretical specific capacity. However, the toxicity and high cost of cobalt represent some of the problems of this material. Thus, extensive research has been carried out over past 10 years to find alternative cathode materials for $LiCoO_2$ in lithium-ion rechargeable batteries. Recently, layer-structured lithium nickel manganese oxides have been shown to be one of the most promising alternative materials for $LiCoO_2$ since their electrochemical and safety characteristics are comparable or better than $LiCoO_2$ [1,2]. These materials contain alternating predominantly lithium layers, and layers containing Mn^{4+}, Ni^{2+}, and, for $x < 0.5$, Li^+.

Structural properties are strongly related to the electrochemical performance of cathode materials and hence, powder X-ray diffraction (XRD) has been widely used to study these materials. Synchrotron-based high resolution in situ XRD has been demonstrated to be a powerful tool to study the structural changes during charge and discharge [3]. However, the information obtained from XRD data is limited to long-range structural order and XRD is not very sensitive to light elements, such as lithium. Recently, ^{6}Li MAS NMR spectroscopy has been applied to examine the variations in local structure of lithium manganate cathode materials for Li rechargeable batteries [4,5]. ^{6}Li MAS NMR spectroscopy is an excellent technique for characterizing local structure in cathode materials with or without long-range order. In this work, the effect of Li deintercalation on the layer-structured lithium nickel manganese oxide, $Li[Li_{1/9}Ni_{3/9}Mn_{5/9}]O_2$ has been systematically investigated by using in situ XRD, EXAFS, and ^{6}Li MAS NMR spectroscopy.

2. Experimental

$Li[Li_{1/9}Ni_{3/9}Mn_{5/9}]O_2$ powders were synthesized by reacting stoichiometric quantities of a coprecipitated double hydroxide of manganese and nickel with lithium hydroxide at 900 °C for 24 h in O_2. The concentration of lithium ions in the transition metal layer was confirmed by quantitative analysis of NMR peak areas (see later). Cathode specimens were prepared by mixing the $Li[Li_{1/9}Mn_{5/9}Ni_{3/9}]O_2$ powders with 10 wt.% acetylene black and 10 wt.% poly-vinylidene fluoride (PVDF) in *n*-methyl pyrrolidone (NMP) solution. 1 M $LiPF_6$ in a 1:1 ethyl carbonate:dimethyl carbonate (EC:DMC) solution was used as the electrolyte. The cell was assembled in an argon-filled glove box. The cells were disassembled for the NMR experiments and the electrodes were washed with tetrahydrofuran prior to packing the samples into the NMR rotors.

* Corresponding author. Tel.: +1-631-632-9548.
E-mail address: cgrey@sbchem.sunysb.edu (C.P. Grey).

0378-7753/03/$ – see front matter © 2003 Elsevier Science B.V. All rights reserved.
doi:10.1016/S0378-7753(03)00195-2

In situ XRD spectra were collected on beam line X18A (using a wavelength, λ of 1.195 Å) at the National Synchrotron Light Source (NSLS) located at Brookhaven National Laboratory. The step size of the 2θ scan was 0.02° in the regions with Bragg reflections and 0.05° in the regions without reflections. The XRD patterns were collected in transmission mode. EXAFS measurements were performed in the transmission mode at beamline 18B of the NSLS using a Si(1 1 1) double-crystal monochromator detuned to 35–45% of its original intensity to eliminate the high order harmonics. Energy calibration was carried out using the first inflection point of the spectrum of Mn and Ni metal foil as a reference (i.e. Mn K-edge = 6539 eV and Ni K-edge = 8333 eV). ^{6}Li MAS NMR experiments were performed at 29.47 MHz on a CMX-200 spectrometer with a double resonance probe built by Samoson and coworkers equipped with 2 mm rotors for MAS. Spin-echoes ($90° - \tau - 180° - \tau -$ acq) were used to acquire the spectra. The sequence was rotor synchronized, with values of τ being chosen, such that they were equal to the rotor period (i.e. $\tau = 1$/spinning frequency).

3. Results and discussion

The first charge curve is plotted in Fig. 1. The cell was charged at a constant current of 0.16 mA for 47 h to reach the 4.8 V cut-off limit with a specific charge capacity of about 233 mA h/g. However, the charge capacity obtained in the 4.7 V plateau was not completely reversible. This may be due to the decomposition of the electrolyte and/or the degradation of the cathode material. During the first charge, 19 XRD scans were continuously collected, as indicated in Fig. 1. The in situ XRD patterns are plotted in Fig. 2 for the regions with Bragg reflections (indexed based on a hexagonal cell) from 003 to 105, and in Fig. 3 for the Bragg reflections from 107 to 113. The scan numbers marked in Figs. 2 and 3 correspond to the numbers marked on the charging curve in Fig. 1. Each XRD scan took about 2.5 h. In order to make an easy comparison with XRD data collected with Cu Kα radiation, the 2θ angles are converted to those corresponding to a wave length of $\lambda = 1.54$ Å in Figs. 2 and 3. The missing data in part of the scans is due to the X-ray beam being unavailable during this time. Since the charging process continued during this period, the incomplete spectra were retained in the plot. Two hexagonal phases (H1, H2) can be identified and their corresponding Bragg peaks are indexed in Figs. 2 and 3. H2 is clearly visible from scan 7 onwards, and is associated with a slightly larger c-parameter than the H1 phase. Work is currently in progress to explore the effect of charge rates and surface versus bulk effects on the structural changes that occur in this system, by acquiring data with both laboratory and synchrotron X-rays sources (which probe the first few layers and bulk phase, respectively) as a function of the charge rate. No significant changes in the XRD pattern are seen from scans 14 to 19, consistent with the irreversible capacity seen in this part of the charge curve.

Fig. 4 shows the Fourier transform magnitudes of the Mn and Ni K-edge EXAFS spectra of the $Li[Li_{1/9}Ni_{3/9}Mn_{5/9}]O_2$ compounds. The first coordination shell consists of oxygen, while the peak feature due to the second coordination shell is dominated by the nickel and manganese cations. The most significant difference between the Mn and Ni K-edge EXAFS spectra is observed in the second coordination shell. The weaker intensity of the second coordination peak in the Mn data indicates a smaller number of transition metals in the first cation coordination sphere and thus, increased numbers of Li ions. On the basis of the Mn and Ni K-edge EXAFS results, we conclude that the lithium ions in the

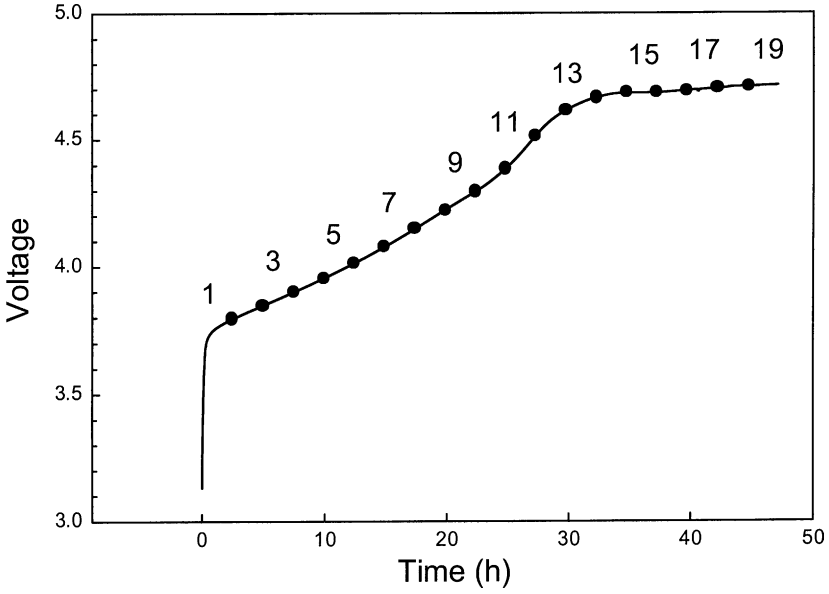

Fig. 1. The fist charge curve of a Li/ $Li[Li_{1/9}Ni_{3/9}Mn_{5/9}]O_2$ cell from 3.0 to 4.8 V at a *C*/47 rate.

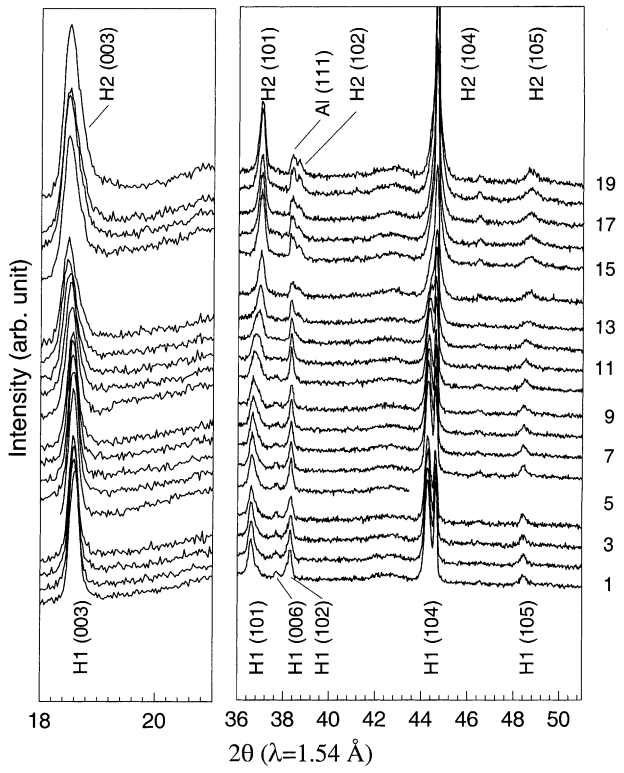

Fig. 2. In situ XRD patterns in the 003 to 105 region of a $Li[Li_{1/9}Ni_{3/9}Mn_{5/9}]O_2$ cathode during the first charge at a *C*/47 rate (2.5 h for each 2θ scan). The 2θ angles have been converted to those corresponding to Cu Kα radiation ($\lambda = 1.54$ Å).

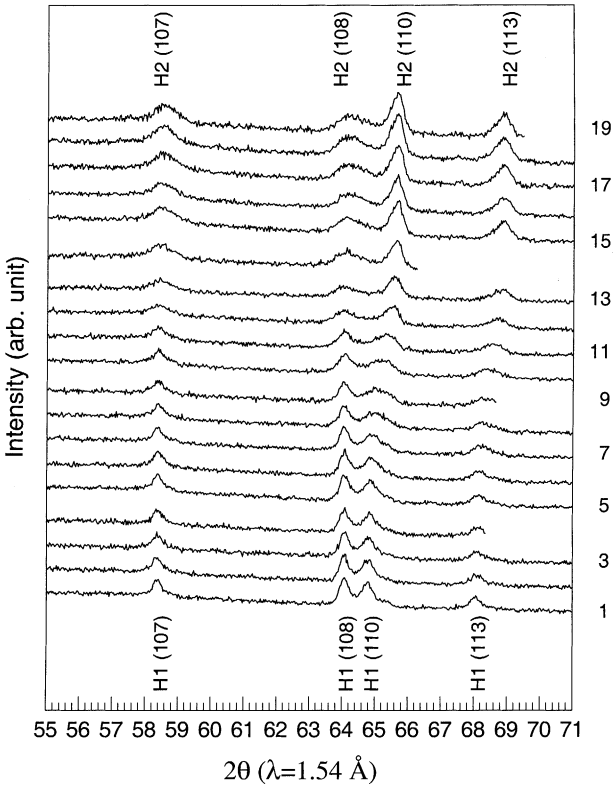

Fig. 3. In situ XRD patterns in the 101 to 113 region of a $Li[Li_{1/9}Ni_{3/9}Mn_{5/9}]O_2$ cathode during the first charge at a *C*/47 rate (2.5 h for each 2θ scan). The 2θ angles have been converted to those corresponding to Cu Kα radiation ($\lambda = 1.54$ Å).

transition metal layers are preferentially surrounded by Mn ions, the material containing Li_2MnO_3-like local environments or domains; this is in good agreement with our NMR results described later.

Fig. 5 shows the ^{6}Li MAS NMR spectra of $Li_{1-x}[Li_{1/9}Ni_{3/9}Mn_{5/9}]O_2$ as a function of state of charge. Two groups of resonances are clearly observed, one at approximately 733–590 ppm and the other at 1498–1324 ppm. The large shifts are ascribed to the hyperfine interaction between the lithium nuclear spins and the unpaired electrons located on the Ni^{2+}/Mn^{4+} ions. Based on our earlier ^{6}Li NMR studies of Li_2MnO_3 and $Li[Li_{0.2}Mn_{0.4}Cr_{0.4}]O_2$, both the shifts and the size and shapes of the spinning sideband manifold of the resonances are consistent with the assignment of these groups of resonances to Li in the predominantly Li layers (733–590 ppm), and Li in the transition metal (Ni^{2+}/Mn^{4+}) layers (1498–1324 ppm) [6,7]. The resonance at 1498 ppm is at a similar chemical shift position to that for Li in the manganese layers in Li_2MnO_3, and is assigned to Li surrounded by six Mn^{4+} ions in the first coordination sphere of cations, i.e. $Li(OMn)_6$. Note that the NMR shifts are consistent with the presence of Mn^{4+} ions and not Mn^{3+}, suggesting that the nickel ions are predominantly present as Ni^{2+}. On this basis, the resonance at 1324 ppm is tentatively assigned to the Li local environment that contains a Ni^{2+} ion in the first coordination sphere [8]. Lithium in the lithium layers of Li_2MnO_3 resonates at approximately 700 ppm. The much broader resonance observed for $Li[Li_{1/9}Ni_{3/9}Mn_{5/9}]O_2$, also at approximately 733 ppm, is ascribed to the large number of different local environments for Li in the Li layers, that result from the presence of Ni^{2+}, Mn^{4+} and Li^+ ions in the first and second cation coordination spheres surrounding the lithium ions. Based on the nature of the overlap expected between the 1/2-filled Ni^{2+} e_g orbitals and the lithium 2s orbitals (via the oxygen orbitals), we tentatively ascribe the shoulders to higher and lower frequencies of the 733 ppm resonance to lithium environments that contain large numbers of Ni^{2+} ions in the second and first cation coordination spheres, respectively (i.e. Li environments that interact with Ni^{2+} via so-called 180 and 90° Li–O–Ni interactions).

The results indicate that lithium ions replace some of the transition metals in the predominantly Ni^{2+}/Mn^{4+} layers. The lithium substitution into the transition metal layers is ascribed to the strong coulombic driving force for charge ordering of 1^+ and 4^+ cations on a trigonal lattice, when they are present in a 1:2 ratio, as occurs in, for example, Li_2MnO_3. This should be contrasted to the charge ordering process for Ni^{2+} and Mn^{4+} ions, which is associated with a smaller energy [9].

On charging, Li ions in both the Mn^{4+}/Ni^{2+} and lithium layers are removed and no new resonances are observed.

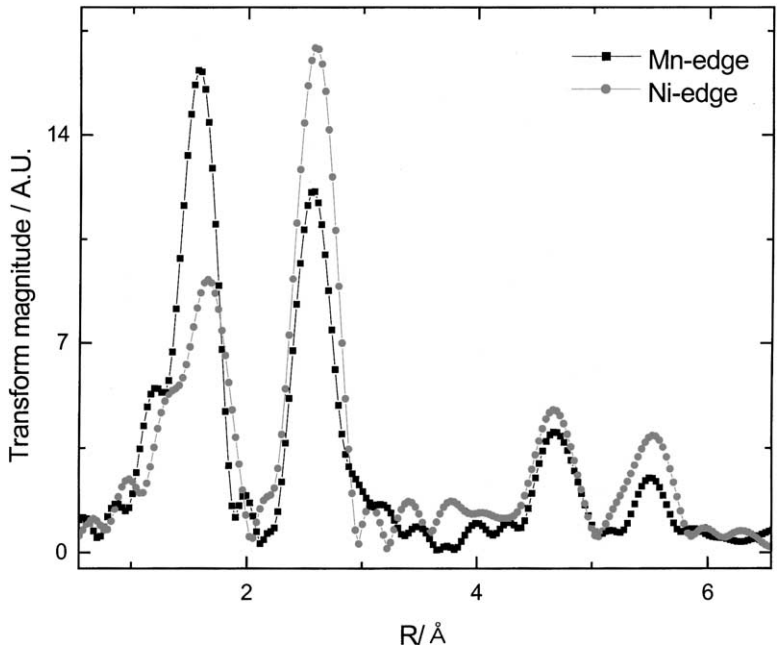

Fig. 4. Fourier transform magnitudes of the Mn and Ni K-edge EXAFS spectra of $Li[Li_{1/9}Ni_{3/9}Mn_{5/9}]O_2$ compounds.

Only the resonance due to Li in the lithium layers at ~570 ppm is observed for the 231 mA h/g charged sample. This behavior is dramatically different from that of $Li[Li_{0.2}Mn_{0.4}Cr_{0.4}]O_2$ where the resonances at approximately 1400 and 700 ppm, due to the Li_2MnO_3 domains in the solid, remain while the Li^+ ions in the Mn^{4+}-doped $LiCrO_2$ regions are removed. The resonance at 570 ppm contains relatively few spinning sidebands, and, based on the larger magnetic susceptibility of the $S = 3/2$ Mn^{4+} ions, in comparison to the $S = 1$ Ni^{2+} and $S = 0$ Ni^{4+} ions, cannot be due to lithium in an octahedral site with predominantly Mn^{4+} ions in the first cation coordination sphere. Thus, the lithium that remains in the lattice at higher potentials appears to be predominantly nearby nickel. Finally, Li in the transition metal layers in environments such as $Li(OMn)_6$ is readily removed, even though this process must involve the oxidation of a more distant transition metal ion. This is consistent with our results for $Li(NiMn)_{0.5}O_2$ [8].

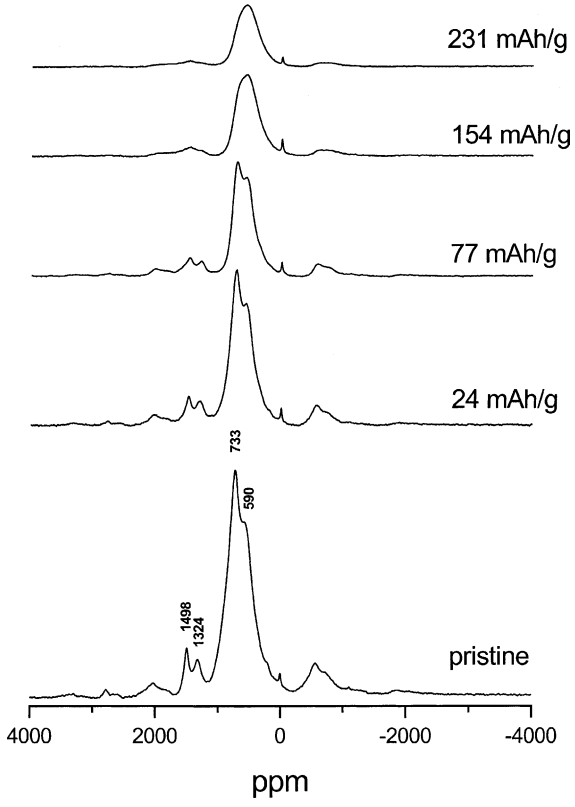

Fig. 5. ^6Li MAS NMR spectra of $Li_{1-x}[Li_{1/9}Ni_{3/9}Mn_{5/9}]O_2$ as a function of state of charge. All spectra were acquired with spinning speeds of 38 kHz.

4. Conclusion

The variations in the structures of the $Li[Li_{1/9}Ni_{3/9}Mn_{5/9}]O_2$ electrode during the first charge process have been investigated by using in situ XRD, EXAFS, and ^6Li MAS NMR techniques. In situ XRD results show that the c-parameter for the $Li[Li_{1/9}Ni_{3/9}Mn_{5/9}]O_2$ material increases only slightly during charge. From the observation of EXAFS results, it is found that the $Li[Li_{1/9}Ni_{3/9}Mn_{5/9}]O_2$ compound contains localized clusters of Li_2MnO_3 and lithium nickel/manganese oxide. The ^6Li MAS NMR results of $Li_{1-x}[Li_{1/9}Ni_{3/9}Mn_{5/9}]O_2$ at different charge states reveal that Li is found not only in the Li layer but also in the Ni^{2+}/Mn^{4+} layers, primarily in an environment surrounded by six Mn^{4+} as in Li_2MnO_3; this is in agreement with the EXAFS results. All the Li^+ ions in the Ni^{2+}/Mn^{4+} layers are

removed on charging, the residual Li^+ occupying sites near nickel in the lithium layers.

Acknowledgements

The work performed at SUNY Stony Brook was supported by the Assistant Secretary for Energy Efficiency and Renewable Energy, Office of Freedom CAR and Vehicle Technologies of the US Department of Energy under Contract No. DE-AC03-76SF00098, via subcontract No. 6517749 with the Lawrence Berkeley National Laboratory. The work carried out at BNL was supported by the Assistant Secretary for Energy Efficiency and Renewable Energy, Office of Transportation Technologies, Electric and Hybrid Propulsion Division, USDOE under Contract Number DE-AC02-98CH10886.

References

[1] Z. Lu, D.D. MacNeil, J.R. Dahn, Electrochem. Solid State Lett. 4 (2001) A191.
[2] T. Ohzuku, Y. Makimura, Chem. Lett. (2001) 744.
[3] X.Q. Yang, X. Sun, S.J. Lee, S. Mukerjee, J. McBreen, M.L. Daroux, X.K. Xing, Electrochem. Solid State Lett. 2 (1999) 157.
[4] Y.J. Lee, F. Wang, C.P. Grey, J. Am. Chem. Soc. 120 (1998) 12601.
[5] Y.J. Lee, F. Wang, S. Mukerjee, J. McBreen, C.P. Grey, J. Electrochem. Soc. 147 (2000) 803.
[6] C. Pan, Y.J. Lee, B. Ammundsen, C.P. Grey, Chem. Mater. 14 (2002) 2289.
[7] Y.J. Lee, C.P. Grey, J. Phys. Chem. B 106 (2002) 3576.
[8] W.S. Yoon, Y. Paik, X.-Q. Yang, M. Balasubramanian, J. McBreen, C.P. Grey, Electrochem. Solid St. Lett. 5 (2002) A263.
[9] J. Reed, G. Ceder, Electrochem. Solid State Lett. 5 (2002) A145.